Forestry Research

ARTICLE

Open Access

https://doi.org/10.48130/forres-0026-0014

Forestry Research **2026**, 6: e014

PagbZIP60 negatively regulates poplar salt tolerance and carbon assimilation capacity by impairing ROS scavenging and photosynthesis

Wanqi Zhang[1], Yajing Li[1], Hui Dang[1,2], Hui Wang[1], Shuhui Du[1], Tangchun Zheng[3], Juanjuan Huang[4], Kai Zhao[1*] and Shengji Wang[1*]

[1] *Shanxi Key Laboratory of Efficient Cultivation of Forest Resources, College of Forestry, Shanxi Agricultural University, Taigu, Shanxi 030801, China*

[2] *College of Innovation and Entrepreneurship, Shanxi Agricultural University, Taigu, Shanxi 030801, China*

[3] *Beijing Advanced Innovation Center for Tree Breeding by Molecular Design, Beijing Key Laboratory of Ornamental Plants Germplasm Innovation & Molecular Breeding, National Engineering Research Center for Floriculture, Beijing Laboratory of Urban and Rural Ecological Environment, Engineering Research Center of Landscape Environment of Ministry of Education, Key Laboratory of Genetics and Breeding in Forest Trees and Ornamental Plants of Ministry of Education, School of Landscape Architecture, Beijing Forestry University, Beijing 100083, China*

[4] *HuangHuai University, Zhumadian, Henan 463000, China*

* Correspondence: kaizhao@sxau.edu.cn (Zhao K); shengjiwang@sxau.edu.cn (Wang S)

Abstract

Members of the bZIP transcription factor family play critical roles in plant salt adaptation. In this study, transgenic poplar lines with overexpression (OE) and RNA interference (RNAi) mediated suppression of *PagbZIP60* were generated to investigate its function. Under salt stress, OE lines exhibited reduced growth, whereas RNAi lines showed improved performance. Increased superoxide dismutase (SOD) activity, electrolyte leakage rate, Na^+ levels, malondialdehyde and hydrogen peroxide (H_2O_2) contents, but decreased peroxidase (POD) and catalase (CAT) activities, and anthocyanin content were revealed in OE lines compared with those in wild-type poplar (WT). OE lines also presented reductions in leaf number and area, increased stomatal density and aperture, and diminished photosynthetic rate and water utilization efficiency (WUE), leading to a lower capacity for carbon assimilation. PagbZIP60 was found to decrease salt tolerance and carbon sequestration capacity by impairing reactive oxygen species (ROS) scavenging and photosynthesis through negatively regulating the expression of downstream genes (*TT7*, *PMEI*, *MLP*, *SAUR*, and *bZIP61*). This study provides a theoretical and experimental basis for poplar germplasm development with enhanced salt tolerance and improved carbon sequestration capacity.

Keywords: Salt stress, Carbon sequestration, ROS, Poplar, PagbZIP60, Photosynthesis

Citation: Zhang W, Li Y, Dang H, Wang H, Du S, et al. 2026. PagbZIP60 negatively regulates poplar salt tolerance and carbon assimilation capacity by impairing ROS scavenging and photosynthesis. *Forestry Research* 6: e014 https://doi.org/10.48130/forres-0026-0014

Introduction

Plants encounter various abiotic stresses during their growth, such as salt, drought, and extreme temperature stresses, which adversely affect plant growth, development, and productivity[1]. Among these factors, salt stress is a major abiotic stressor that exerts detrimental effects through ion toxicity, osmotic imbalance, and oxidative stress[2]. The combined effects of these mechanisms can lead to stunted plant growth, chlorosis, impaired root development, and ultimately death. Plant salt tolerance is intrinsically linked to carbon sequestration capacity, which reflects the long-term ability of plants to store carbon in biomass. Salt stress not only impairs photosynthesis and carbon assimilation efficiency (the instantaneous CO_2 fixation process), but also reduces carbon sequestration capacity by altering metabolic homeostasis and carbon allocation patterns[3]. In photosynthetic carbon fixation, salt stress primarily affects plants via stomatal and non-stomatal limitation. Stomatal limitation occurs when elevated salinity triggers stomatal closure, leading to decreased CO_2 uptake and reduced photosynthetic rate. In contrast, non-stomatal limitation is characterized by structural damage to chloroplasts and the impairment of essential enzymatic activities[3,4]. For example, salt stress enhances osmotic solute accumulation (e.g., sugars from starch breakdown), but reduces carbon assimilation due to photosynthetic limitations in *Thellungiella halophila*[4].

Salt-tolerant plants can maintain carbon assimilation through several adaptive mechanisms to support long-term carbon sequestration. Osmotic adjustment through proline and compatible solute accumulation preserves cellular hydration, although metabolic costs are simultaneously observed. Ion compartmentalization (e.g., vacuolar Na^+ sequestration) protects chloroplast function and helps sustain photosynthesis. Meanwhile, strategic carbon reallocation enhances belowground carbon storage potential, thereby supporting soil carbon sequestration[5]. Given the increasing severity of global soil salinization and the growing demand to mitigate climate change, the identification of key stress-responsive genes and the development of salt-tolerant plant varieties through genetic engineering have become increasingly prioritized[6–8]. Furthermore, elucidating the molecular mechanisms underlying plant salt stress responses will facilitate the development of strategies to enhance stress tolerance, thereby contributing to food security and environmental sustainability.

The bZIP (basic leucine zipper) transcription factors constitute a conserved protein family that is ubiquitous in eukaryotes. Through their characteristic basic regions and leucine zipper domains, they specifically bind to *cis*-acting elements in promoters of target genes, hence playing important roles in regulating plant responses to environmental stresses[9,10]. The pepper bZIP transcription factor *CaADBZ1* is induced by dehydration and exogenous abscisic

acid (ABA), and enhances plant drought tolerance through ABA-dependent pathways. Specifically, *CaADBZ1* overexpression strengthens ABA signaling and activates dehydration-responsive genes, improving plant survival under water-deficit conditions[11]. *PmbZIP31/36/41* are markedly upregulated during freezing stress, but respond weakly to chilling stress, demonstrating functional divergence in cold adaptation in *Prunus mume*[12]. *Arabidopsis* NAC transcription factor ANAC096 interacts with ABF/AREB-type bZIP transcription factors to coactivate ABA-responsive genes. This synergistic regulation strengthens ABA signaling pathways and enhances plant survival under osmotic stresses such as drought and salinity[13]. Although numerous studies in poplar have focused on identifying members of the bZIP gene family and analyzed their expression patterns, their regulatory roles in salt stress responses remain poorly understood[14,15]. In particular, few studies have examined the relationship between bZIP genes and carbon sequestration capacity in poplar, or the mechanisms by which bZIP regulates salt tolerance through reactive oxygen species (ROS) scavenging. Elucidating these mechanisms is therefore essential for developing poplar genotypes that can tolerate salt stress without compromising carbon assimilation capacity; traits that are critical for afforestation and sustainable bioenergy production.

Populus species are fast-growing and ecologically adaptable trees, widely used in plantation forests worldwide. As a vital renewable resource, they provide timber and bioenergy feedstock while also supporting landscape restoration through afforestation. Their high biomass productivity contributes significantly to carbon sequestration in terrestrial ecosystems. However, poplars are sensitive to environmental stresses such as salinity and drought. Soil salinization represents a major abiotic stress that severely limits poplar growth and biomass productivity. Therefore, elucidating the molecular mechanisms of salt stress responses in poplar is critical for advancing fundamental knowledge and providing a theoretical basis for developing novel poplar varieties with enhanced carbon assimilation capacity. Our previous study indicated that members of the bZIP gene family played important roles in regulating poplar growth, development, and salt stress responses through distinct gene networks or biological processes. Some members may also respond to salt or osmotic stress by regulating ion balance[14]. Although AtbZIP60 mediates cellular salt stress responses in *Arabidopsis*, the function of its poplar ortholog (PagbZIP60) in growth, development, and stress resistance remains largely uncharacterized[16]. In this study, we identified the salt-induced gene *PagbZIP60* and generated transgenic poplar lines with either overexpression or RNA interference (RNAi)-mediated suppression of *PagbZIP60*. Physiological and biochemical analyses demonstrated that PagbZIP60 negatively modulates salt tolerance and carbon assimilation capacity by impairing key physiological processes, including ROS scavenging and photosynthesis. This work provides a molecular basis for developing salt-tolerant poplar varieties, facilitates the afforestation of saline-alkali lands, and enhances carbon sequestration in plantation forests.

Materials and methods

Plant materials and growth conditions

Both the 84K poplar (*Populus alba* × *P. glandulosa*) and *Nicotiana benthamiana* used in this study were grown under controlled conditions in the Forest Tree Genetics and Breeding Laboratory at Shanxi Agricultural University. Growth parameters were maintained as follows: temperature at 25 °C, a 16 h light/8 h dark photoperiod, and relative humidity at 60%−70%.

To investigate the function of PagbZIP60 in response to salt stress, one-month-old tissue-cultured saplings (non-transgenic and transgenic) were first acclimated in a hydroponic system containing distilled water for an additional month. They were then transplanted into pots and grown in a greenhouse for 45 d. Previous studies show that 150 mM NaCl imposes significant salt stress on poplar seedlings without causing immediate lethality[17,18]. Therefore, plants were treated with 150 mM NaCl solution (N-group) for 10 d, while controls received distilled water (C-group). Root, stem, and leaf tissues were separately harvested, flash-frozen in liquid nitrogen, and stored at −80 °C for further analysis.

Gene cloning and poplar genetic transformation

Total RNA was extracted from 84K poplar leaves using the RNAprep Pure Plant Kit (Tiangen Biotech, Beijing), following the manufacturer's instructions. cDNA was synthesized, and *PagbZIP60* (GenBank number PX842721) was cloned based on the homologous *PtrbZIP60* (*Potri.005G257900*) transcript sequence retrieved from the Phytozome database (https://phytozome-next.jgi.doe.gov/). Primers bZIP60-F/R, synthesized by Tsingke Biotech (Beijing, China), were used for amplification (Supplementary Table S1).

For the *PagbZIP60* overexpression vector, the pBI121-GFP vector was digested with *Sma* I and *Spe* I enzymes, and then ligated with the *PagbZIP60* fragment (amplified using primers PagbZIP60-121-F/R) to generate the recombinant pBI121-PagbZIP60-GFP construct (Supplementary Fig. S1a). A BLAST-verified, unique fragment of PagbZIP60, lacking conserved domains, was selected as the RNAi target to ensure specificity. The sense fragment was cloned into pROKII via *Xba* I and *Sma* I restriction sites, while the antisense fragment was inserted using *Spe* I and *Sac* I sites (Supplementary Fig. S1b) yielding the final pROKII-RNAi-PagbZIP60 recombinant vector. Both the *PagbZIP60* overexpression (OE) and RNAi recombinant vectors were successfully transferred into *Agrobacterium tumefaciens* strain EHA105 via the freeze-thaw method. Transgenic poplar lines with either *PagbZIP60* overexpression or suppression were generated through *Agrobacterium*-mediated leaf disc transformation. Positive transgenic lines were selected on 1/2 Murashige and Skoog (MS) medium containing 50 mg/L kanamycin, and transgenic lines were validated by PCR and RT-qPCR.

Protein alignment and tertiary structure

Amino acid sequences of PagbZIP60 homologs were identified by BLAST searches and downloaded from NCBI (https://ncbi.nlm.nih.gov/). Multiple sequence alignment was conducted using the ClustalW algorithm implemented in BioEdit 7.0.9.1 with default parameters, and the protein tertiary structure was predicted by homology modeling using SWISS-MODEL (https://swissmodel.expasy.org/).

RNA extraction and RT-qPCR

Leaves from transgenic poplar lines were harvested for RNA extraction. RT-qPCR analysis was performed using the CFX Duet Real-Time PCR System (Bio-Rad, California, USA) and SuperReal PreMix Kit (SYBR Green, Tiangen, Beijing, China). The expression level of each transcript was normalized to internal reference genes *Actin* and *UBQ* in each sample. The relative expression of the target gene was quantified via the $2^{-\Delta\Delta C_T}$ method[19]. The primers used in this study are listed in Supplementary Table S1.

Subcellular localization

To determine the subcellular localization of the PagbZIP60 protein, the pBI121-PagbZIP60-GFP vector containing the 35S promoter and the full coding sequence of *PagbZIP60* was prepared. The 35S:mKATE-NLS vector fused with a nuclear localization signal (NLS) was used as a nuclear marker[20]. *Agrobacterium tumefaciens* strains carrying pBI121-*PagbZIP60*-GFP or 35S:GFP (control) were each mixed with the 35S:mKATE-NLS strain at a 1:1 ratio. The mixtures were then infiltrated into *Nicotiana benthamiana* leaves. After 48 h incubation in darkness, fluorescence signals were examined under a confocal microscope (Olympus FV1000, Japan) to visualize the PagbZIP60-GFP fusion protein localization.

Transcriptional activation activity

To assess transcriptional activation activity, *PagbZIP60* was cloned into the pGBKT7 vector using *Eco*R I and *Sal* I restriction sites with primers *PagbZIP60*-BD-F/R (Supplementary Table S1). The recombinant pGBKT7-PagbZIP60, empty pGBKT7, and positive control plasmids (pGBKT7-53/pGADT7-T co-transformed plasmids) were individually transformed into the Y2HGold yeast strain. Transformed yeast cells were plated on SD/-Trp, and SD/-Trp/-His/-Ade/X-α-Gal media to evaluate their growth phenotypes[21].

Morphological indicators

Morphological traits of transgenic and wild-type (WT) 84K poplar lines were quantified. Plant height was measured with a ruler, and basal stem diameter was measured with a vernier caliper. Leaf length and width were measured using a leaf area scanner (TOP CloudAgri, Zhejiang, China). Roots were scanned with an Epson Perfection V750 Pro scanner (Epson, China), and parameters (length, diameter, area, volume) were analyzed using WinRHIZO software (Regent Instrument, Canada). At least six biological replicates per line were used to ensure experimental reliability.

Photosynthesis-related Indicators

Between 9:00 and 11:00 a.m., the 3rd to 5th leaves of each plant were selected for photosynthetic measurement using an infrared gas analyzer (LI-6400; LI-COR, Lincoln, NE, USA). Parameters were set as follows: leaf temperature at 25 °C, photosynthetically active radiation (PAR) at 1,500 μmol/(m^2·s), and a flow rate of 500 μmol/s[22]. Net photosynthetic rate (Pn, μmol/[m^2·s]), stomatal conductance (Gs, mmol/[m^2·s]), and transpiration rate (Tr, mmol/[m^2·s]) were recorded. Instantaneous water utilization efficiency (WUE) was calculated as the ratio of Pn to Tr (WUE = Pn/Tr, μmol/mmol). Six biological replicates per treatment were used to ensure data reliability.

Stress-related physiological indicators

The activities of enzymes, including superoxide dismutase (SOD), peroxidase (POD), and catalase (CAT), as well as the contents of malondialdehyde (MDA), soluble sugars, soluble proteins, and anthocyanins in plant leaves were measured spectrophotometrically before, and after stress treatment. SOD, POD, and CAT activities were determined using established spectrophotometric methods based on NBT photoreduction inhibition, guaiacol oxidation, and hydrogen peroxide (H_2O_2) decomposition, respectively, while MDA content was quantified using the thiobarbituric acid (TBA) method. Soluble sugars, soluble proteins, and anthocyanins were measured according to standard colorimetric methods. Leaf relative electrical conductivity was quantified with a conductivity meter. Relative electrolyte leakage (%) was calculated as the ratio of initial to total conductivity after boiling. Proline and H_2O_2 contents were assayed using kits (Nanjing Jiancheng Bioengineering Institute, China). Superoxide anion (O_2^-) content was determined with a kit (Beijing Solarbio Science & Technology Co., Ltd., China), following the manufacturer's instructions. Hydrogen peroxide accumulation was cross-validated by 3,3'-diaminobenzidine (DAB) histochemical staining. Brown precipitates indicate *in situ* H_2O_2 accumulation in leaf tissues.

Na^+ and K^+ content

Leaves were rinsed with distilled water, dried, and enzyme-inactivated at 105 °C. After drying at 65 °C to constant weight, 2.5 g samples were weighed into polytetrafluoroethylene digestion tubes. Then, 5 mL of concentrated nitric acid (HNO_3, 65%–68%) and 2 mL of hydrogen peroxide (H_2O_2, 30%) were added, followed by vortex mixing. Digestion proceeded with sequential temperature ramping: 100 °C (60 s) to 140 °C (60 s), and finally to 180 °C (10 min). Digests were diluted to 50 mL with deionized water, filtered through Whatman filter membranes and analyzed for Na^+/K^+ using the NovAA400P atomic absorption spectrometer (Analytik Jena, Germany)[23].

Carbon sequestration capacity

Plants assimilate atmospheric CO_2 (inorganic carbon) into organic carbon (e.g., glucose, cellulose) via photosynthesis. This organic carbon constitutes plant biomass (cell walls, starch, lipids) and serves as energy storage. To assess carbon sequestration capacity, we quantified total organic carbon (TOC) in poplar. Terminal buds were subcultured for 35 d in 1/2 MS medium containing 0 or 50 mM NaCl (20 biological replicates per line). Uniformly vigorous plants were subjected to enzyme inactivation (105 °C, 15 min), drying (80 °C to constant weight), and ball-mill grinding. Samples were acid-washed (1 M HCl, 24 h) to remove inorganic carbon. Aliquots (10 mg) were combusted at 850 °C for 5 min in preheated furnaces. TOC content was determined using a Multi N/C 2100 analyzer (Analytik Jena AG, Germany) with Potassium Hydrogen Phthalate (KHP) standards (0–1,000 mg C/L) and quartz crucible blanks[24].

Stomatal morphology

Apical shoots with 2–3 leaves were excised and rooted in medium containing 0 or 50 mM NaCl for one month. Then the abaxial surface of mature functional leaves was coated with nail polish. Stomatal impressions were transferred using transparent adhesive tape to prepare temporary slides[25]. Slides were examined under an Olympus CX31RTSF microscope (Japan), and stomatal density and aperture of open stomata were quantified with ImageJ software[26]. For stomatal aperture measurement, the width of the stomatal pore (transverse aperture) of fully expanded open stomata was measured in randomly selected microscopic fields. Stomatal density was calculated as the number of stomata per unit leaf area (stomata/mm^2) by counting three randomly selected fields per leaf using ImageJ software. Twelve biological replicates per line were used to ensure experimental accuracy.

Fiber cell length

Stem segments (7th nodes, 1cm) from transgenic and WT plants were sectioned. Segments were incubated in 30% H_2O_2: glacial

acetic acid (1:1 v/v) at 60 °C for 24–36 h. After rinsing with deionized water, samples were stained with 0.1% safranine O. Fiber cell lengths in secondary xylem were measured using an Olympus CX31RTSF microscope (Japan) with ImageJ software, analyzing ≥ 12 biological replicates per line[27].

RNA-seq

Total RNA was extracted from leaves of 35-d-old OE and WT plants (n = 3 biological replicates). RNA integrity (Supplementary Table S2) was assessed using a Qsep400 High-throughput Biological Fragment Analyzer (Taiwan, China). Libraries (insert size: 250–350 bp) were sequenced on the BGI platform by Metware Biotechnology Co. (Wuhan, China)[28]. Each sample yielded ≥ 6 Gb of clean data (total 46.15 Gb), with Q30 ≥ 94%, and GC content of 40%–60%. Clean reads were aligned to the *Populus trichocarpa* v4.1 reference genome (JGI: https://genome.jgi.doe.gov/portal/pages/dynamicOrganismDownload.jsf?organism=Ptrichocarpa) using the HISAT2 software[29]. The overall mapping rate ranged from 77.24% to 77.66%, with unique mapping rates between 75.25% and 75.63% across all samples. Genes with an adjusted $|\log_2(\text{FoldChange})| \geq 1$ and an FDR < 0.05, as determined by DESeq2, were classified as differentially expressed genes (DEGs)[30]. The FPKM (fragments per kilobase of transcript per million mapped reads) values for each gene were calculated based on its length and the number of reads mapped to it. Using the clusterProfiler software, we performed GO (Gene Ontology) term, and KEGG (Kyoto Encyclopedia of Genes and Genomes) pathway enrichment analyses on the set of DEGs[31]. A significance threshold of $padj < 0.05$ was applied.

Twenty non-transgenic 84K soil-grown seedlings (60 d old with uniform growth status) were subjected to 150 mM NaCl for 24 h. Roots, stems, leaves, and buds were separately harvested for transcriptome sequencing to examine the expression patterns of target genes.

Yeast one-hybrid assay

The *PagbZIP60* coding sequence was directionally cloned into pGADT7-Rec2 in-frame with the GAL4 activation domain, generating the prey fusion protein[32]. For bait construction, a triple-repeat conserved *cis*-element was synthesized and inserted into the pHis2 vector upstream of the minimal promoter. Prey and bait plasmids were cotransformed into Y187 yeast cells. In this yeast one-hybrid (Y1H) system, binding of the PagbZIP60-GAL4 activation domain fusion protein to the *cis*-element recruits the transcriptional apparatus to the minimal promoter, thereby activating the *HIS3* reporter gene. Yeast growth on histidine-deficient selective media supplemented with an appropriate concentration of 3-amino-1,2,4-triazole (3-AT) directly reflects the protein-DNA interaction, providing a functional readout of the binding specificity of PagbZIP60 to the target *cis*-element. Y1H assays followed the manufacturer's protocol (Y187-pHis2 Interaction Validation Kit, Coolaber, China).

Dual luciferase reporter assay

The full-length coding sequence of *PagbZIP60* was cloned and ligated into the effector vector pGreenII 62-SK, while 5× tandem copies of *cis*-elements were tandemly inserted into the reporter vector pGreenII 0800-LUC. The constructs were transformed into *Agrobacterium* strains GV3101 and co-infiltrated into *Nicotiana benthamiana* leaves. After 72 h, the LUC signals were detected with a luminescence imaging system[33]. Following the measurement of FLUC and RLUC activities using the Dual Luciferase Reporter Gene Assay Kit (Coolaber, China), relative luciferase activity was calculated as the FLUC/RLUC ratio[17]. The values were normalized to the control group, and the data was expressed as normalized relative luciferase activity.

Promoter motif analysis

The presence of ABRE *cis*-regulatory elements in the promoters of candidate genes was analyzed using the Basic Biosequence View tool in TBtools (v2.0) with its built-in motif database. The 2,000 bp sequence upstream of the translation initiation codon of PagbZIP60 was defined as the promoter region, which was then submitted to the tool for motif scanning with default parameters.

Data analysis

Statistical analyses were performed using GraphPad Prism 9. One-way ANOVA followed by Tukey's HSD test was applied to determine significance among samples, with significance defined at $p < 0.05$.

Results

PagbZIP60 exhibited salt-responsive and tissue-specific expression patterns

To characterize the expression pattern of *PagbZIP60*, RNA-seq was performed on 60-d-old non-transgenic 84K poplar seedlings subjected to 150 mM NaCl. Under control conditions, *PagbZIP60* displayed tissue-specific expression, with the highest expression level in roots and the lowest in buds. Under salt stress, *PagbZIP60* was significantly induced in buds, leaves, and stems (Fig. 1a). RT-qPCR result demonstrated that *PagbZIP60* was also significantly upregulated in roots under salt stress (Fig. 1b). In summary, *PagbZIP60* was induced by salt stress in a tissue-specific manner, with the strongest expression observed in buds and leaves.

To further elucidate the biological function of PagbZIP60, we cloned the *PagbZIP60* gene from 84K poplar leaves. The full-length coding sequence (CDS) of *PagbZIP60* comprised 921 base pairs, encoding a protein of 306 amino acids (Supplementary Fig. S2a). Notably, it exhibited a high similarity to PtrbZIP60 (XP_002307824) from *P. trichocarpa*, with only one amino acid difference in the conserved bZIP domain (Fig. 1c, d). Furthermore, the tertiary structure of PagbZIP60 primarily consisted of random coils and α-helices, and contained a conserved bZIP_HY5-like domain (Supplementary Fig. S3). Transcriptional activation analysis in yeast cells revealed that the PagbZIP60 protein did not exhibit transcriptional activation activity in yeast (Fig. 1e). PagbZIP60 was predominantly localized in the nucleus and cytoplasm, as determined by transient expression of a GFP fusion protein in tobacco leaves (Fig. 1f).

PagbZIP60 inhibited poplar growth and development

The *Agrobacterium*-mediated leaf disc transformation method was employed to generate transgenic poplar lines overexpressing or suppressing *PagbZIP60* (Supplementary Fig. S2b, S2c). The positive transgenic lines were confirmed using PCR and RT-qPCR techniques at both the DNA and RNA levels. The results of these analyses revealed the successful generation of three *PagbZIP60* overexpression lines (Supplementary Fig. S2d, S2e) and three RNAi lines, respectively (Supplementary Fig. S2f, S2g). Based on significant differences in *PagbZIP60* expression levels compared to the WT,

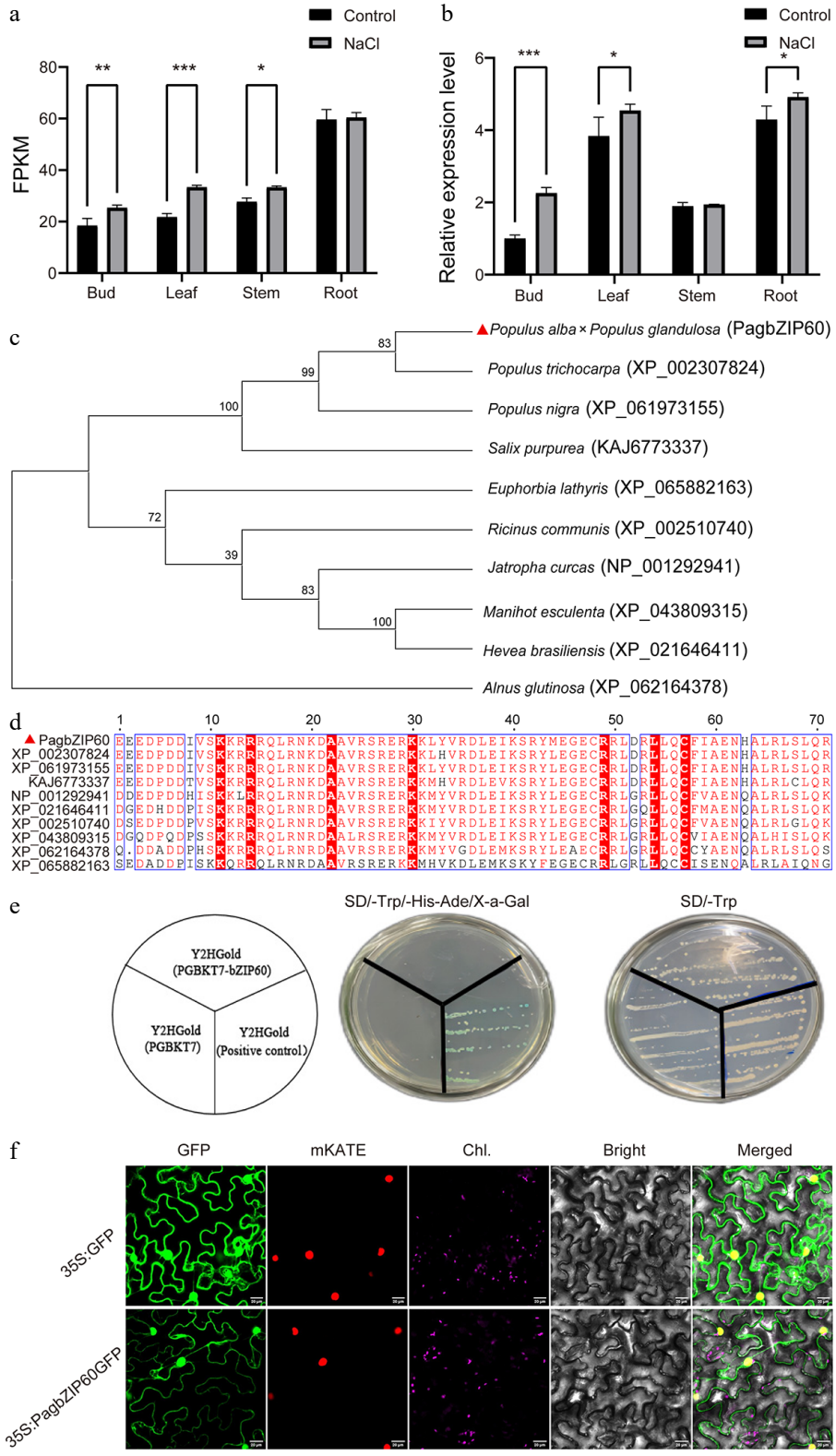

Fig. 1 Gene expression and protein characterization of PagbZIP60. (a) Expression pattern of *PagbZIP60* in different tissues of poplar under 150 mM NaCl, detected by RNA-seq. The stars indicate significant differences between samples, * $p < 0.05$, ** $p < 0.01$, *** $p < 0.001$. (b) Expression pattern of *PagbZIP60* in different tissues of poplar under 150 mM NaCl, detected by RT-qPCR. (c) Phylogenetic tree of PagbZIP60 and representative plant bZIP proteins. (d) Multiple alignment of the bZIP conserved domain in PagbZIP60. (e) Transactivation assay of PagbZIP60 in yeast cells. (f) Subcellular localization of PagbZIP60 protein in tobacco leaves. GFP: green fluorescence; mKATE: nucleus marker; Chl.: chloroplast marker; Bright: bright field; Merged: merged field; Bar: 20 μm.

two overexpression lines (OE-1 and OE-2) and two RNAi lines (RNAi-1 and RNAi-2) showing the highest overexpression or knockdown efficiency were selected for further investigation.

To investigate the role of PagbZIP60 in poplar growth and development, growth phenotypes of transgenic lines were monitored. One-month-old tissue-cultured seedlings were transplanted into pots following hydroponic acclimation and a 20-d recovery phase. Under these conditions, OE lines exhibited significantly weaker growth, whereas RNAi lines showed enhanced growth compared to WT (Fig. 2a–d). By the 40th d post-transplantation, the plant height, basal stem diameter, and leaf number of OE lines gradually converged toward WT levels. In contrast, the RNAi lines continued to significantly outperform WT, with an approximately two-fold higher leaf number compared to OE lines.

PagbZIP60 amplified salt-induced leaf phenotypes

To assess salt stress response, 45-d-old potted seedlings were subjected to 150 mM NaCl for 10 d. The leaves of the OE lines wilted first, followed by those of WT, whereas leaves of RNAi lines showed minimal wilting or chlorosis (Fig. 3a). No lines exhibited significant increases in height or diameter during the treatment, indicating growth ceases under salt stress (Fig. 3b, c). Furthermore, salt stress caused severe leaf dehydration and shrinkage, which was more pronounced in OE lines (Fig. 3d). Notably, under salt stress, the length and width of OE leaves were significantly reduced compared to non-stressed controls (Fig. 3e, f). These results indicated that *PagbZIP60* overexpression conferred hypersensitivity to salt stress, resulting in pronounced stress-related leaf phenotypes.

To characterize root phenotypes under salt stress, plants were cultured on rooting medium with 50 mM NaCl for 30 d. Under normal conditions, OE lines had significantly greater total root length, surface area, and total volume than those of WT, while no clear pattern was observed between RNAi lines and the WT (Fig. 4a–e). After salt stress, all root parameters declined across lines; however, OE lines maintained significantly higher values than the WT for metrics including average diameter. These findings suggested that *PagbZIP60* overexpression promoted root growth in poplar, even under conditions of short-term salt stress.

PagbZIP60 triggered oxidative damage in leaves

Given the heightened sensitivity of OE line leaves to salt stress, we examined associated changes in physiological and biochemical indicators. Under normal conditions, DAB staining intensity in transgenic plants was comparable to WT, indicating the absence of oxidative stress (Fig. 5a). Under salt stress, OE leaves exhibited significantly higher DAB staining intensity than WT, whereas RNAi leaves showed significantly lower intensity. Furthermore, H_2O_2 and O_2^- contents in OE leaves were 16.50%–21.30%, and 5.79%–9.40% higher, relative to WT; conversely, those in RNAi

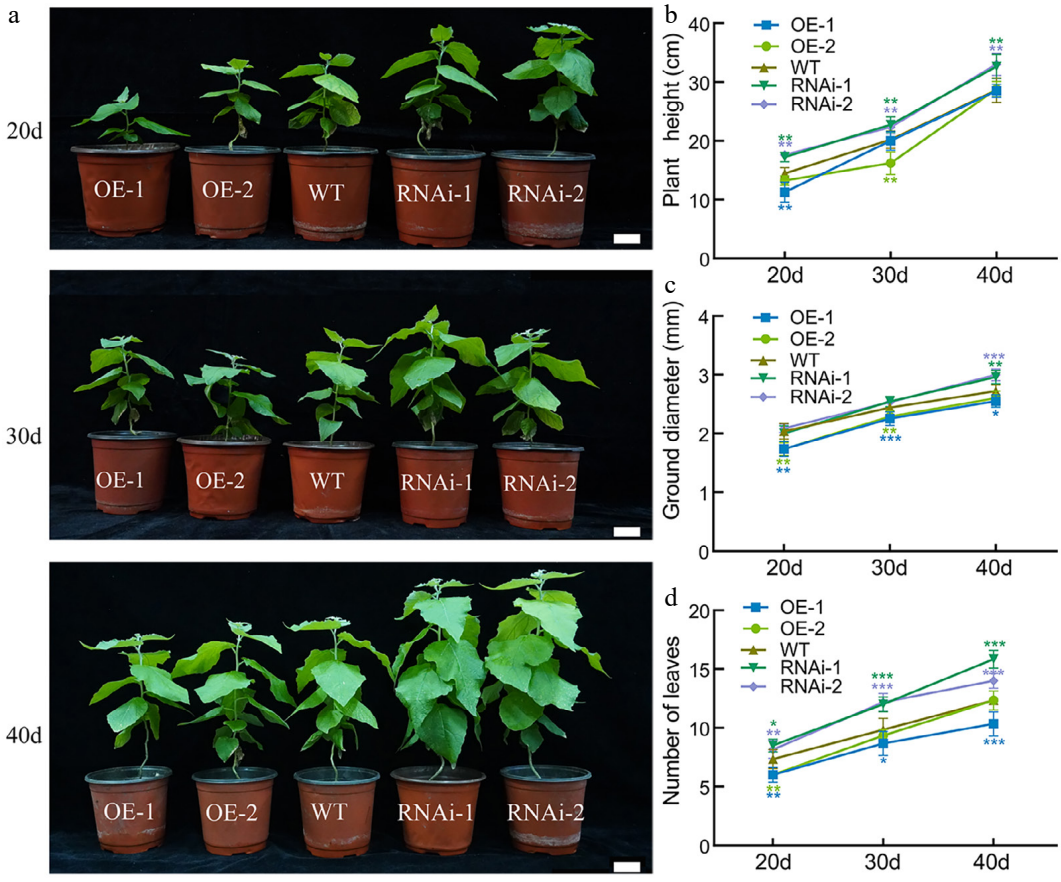

Fig. 2 The growth status of *PagbZIP60* transgenic poplar under normal conditions. (a) The growth status of *PagbZIP60* transgenic poplar under normal conditions. (b) Plant height, (c) ground diameter, and (d) number of leaves of *PagbZIP60* transgenic poplar at different developmental stages. The stars indicate significant differences between *PagbZIP60* transgenic poplar and non-transgenic poplar at the same developmental stage ($p < 0.05$), * $p < 0.05$, * m $p < 0.01$, *** $p < 0.001$. The plot represents the mean ± SD ($n = 6$). OE: *PagbZIP60* overexpression lines, RNAi: *PagbZIP60* suppression lines, WT: non-transgenic poplar. Scale bars, 1 cm.

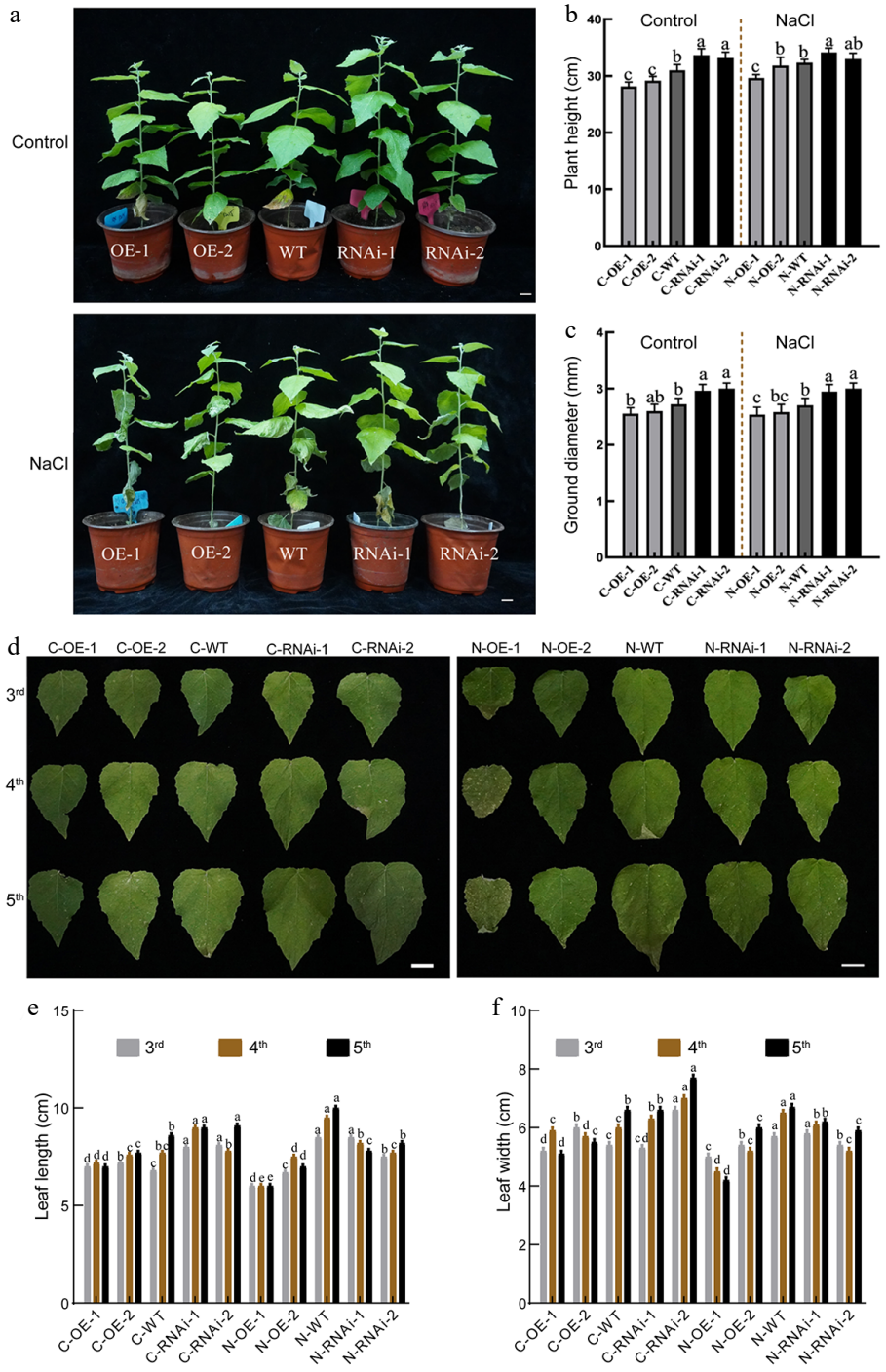

Fig. 3 The growth status of *PagbZIP60* transgenic poplar under salt stress (150 mM NaCl) conditions. (a) The growth status of *PagbZIP60* transgenic poplar. (b) Plant height, and (c) ground diameter of *PagbZIP60* transgenic poplar. (d) The status of mature functional leaves of *PagbZIP60* transgenic poplar. (e) Leaf length, and (f) leaf width of *PagbZIP60* transgenic poplar. The different lowercase letters indicate significant differences among samples ($p < 0.05$). The plot represents the mean ± SD ($n = 6$). OE: *PagbZIP60* overexpression lines, RNAi: *PagbZIP60* suppression lines, WT: non-transgenic poplar, C: normal control growth condition, N: salt stress with NaCl condition. C-OE-1 represents overexpression line 1 under normal conditions; N-OE-1 represents the same line under salt stress. The same nomenclature applies to other abbreviations. Bars: 1 cm.

leaves were 19.50%–27% and 25.39%–27.63% lower compared to WT, respectively (Fig. 5b, c).

Under salt stress, SOD activity and MDA content in OE lines were much higher than those in WT, whereas both parameters were reduced in RNAi lines (Fig. 5d, e). However, POD activity showed the opposite trend to that of SOD and MDA (Fig. 5f). CAT activity (Fig. 5g) and proline content (Fig. 6a) were slightly lower in OE lines under normal conditions, and this disparity increased under salt stress. In contrast, no significant differences were observed in electrolyte leakage or soluble protein content across lines (Fig. 6b, c). Notably, soluble sugar and anthocyanin levels were highest in OE lines under normal conditions, but these showed an opposite pattern under salt stress, with OE lines exhibiting the lowest contents (Fig. 6d, e).

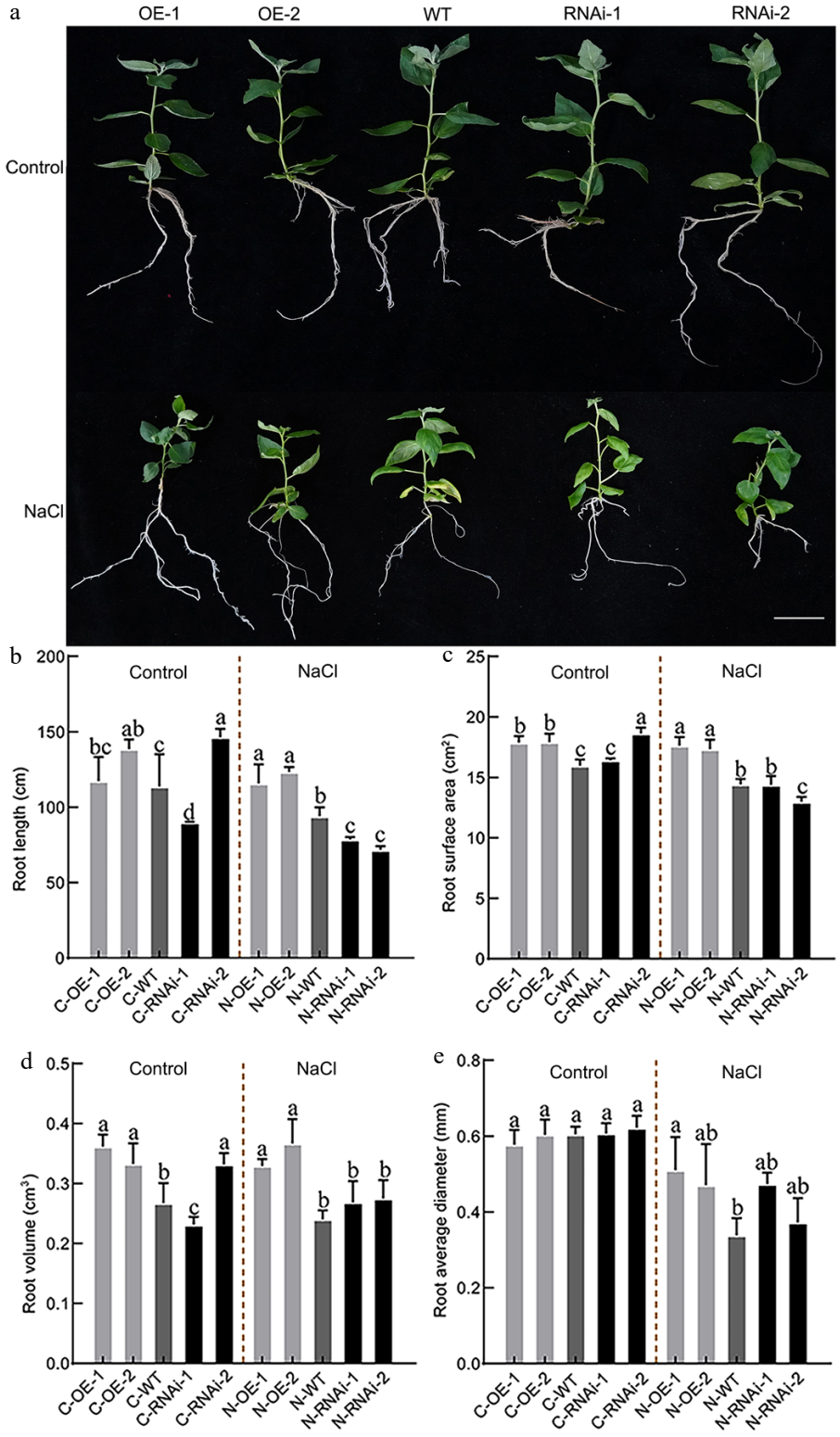

Fig. 4 Root system phenotype analysis of *PagbZIP60* transgenic poplar under salt stress. (a) The root status of *PagbZIP60* transgenic poplar grown in the 1/2 MS medium containing 50 mM NaCl for 30 d. (b) Total root length, (c) root surface area, (d) root volume, and (e) average diameter of *PagbZIP60* transgenic poplar in the 1/2 MS media containing 50 mM NaCl for 30 d. The different lowercase letters indicate significant differences among samples ($p < 0.05$). The plot represents the mean ± SD ($n = 6$). OE: *PagbZIP60* overexpression lines, RNAi: *PagbZIP60* suppression lines, WT: non-transgenic poplar, C: normal control growth condition, N: salt stress with NaCl condition. C-OE-1 represents overexpression line 1 under normal conditions; N-OE-1 represents the same line under salt stress. The same nomenclature applies to other abbreviations. Bars: 1 cm.

PagbZIP60 disrupted K^+/Na^+ homeostasis

The balance between K^+ and Na^+ contents is crucial for cellular osmotic regulation and water retention in plants. Under normal conditions, OE lines showed the highest Na^+ content, whereas RNAi lines displayed the lowest (Fig. 6f). Upon salt stress, Na^+ content increased significantly in all lines with OE lines maintaining the

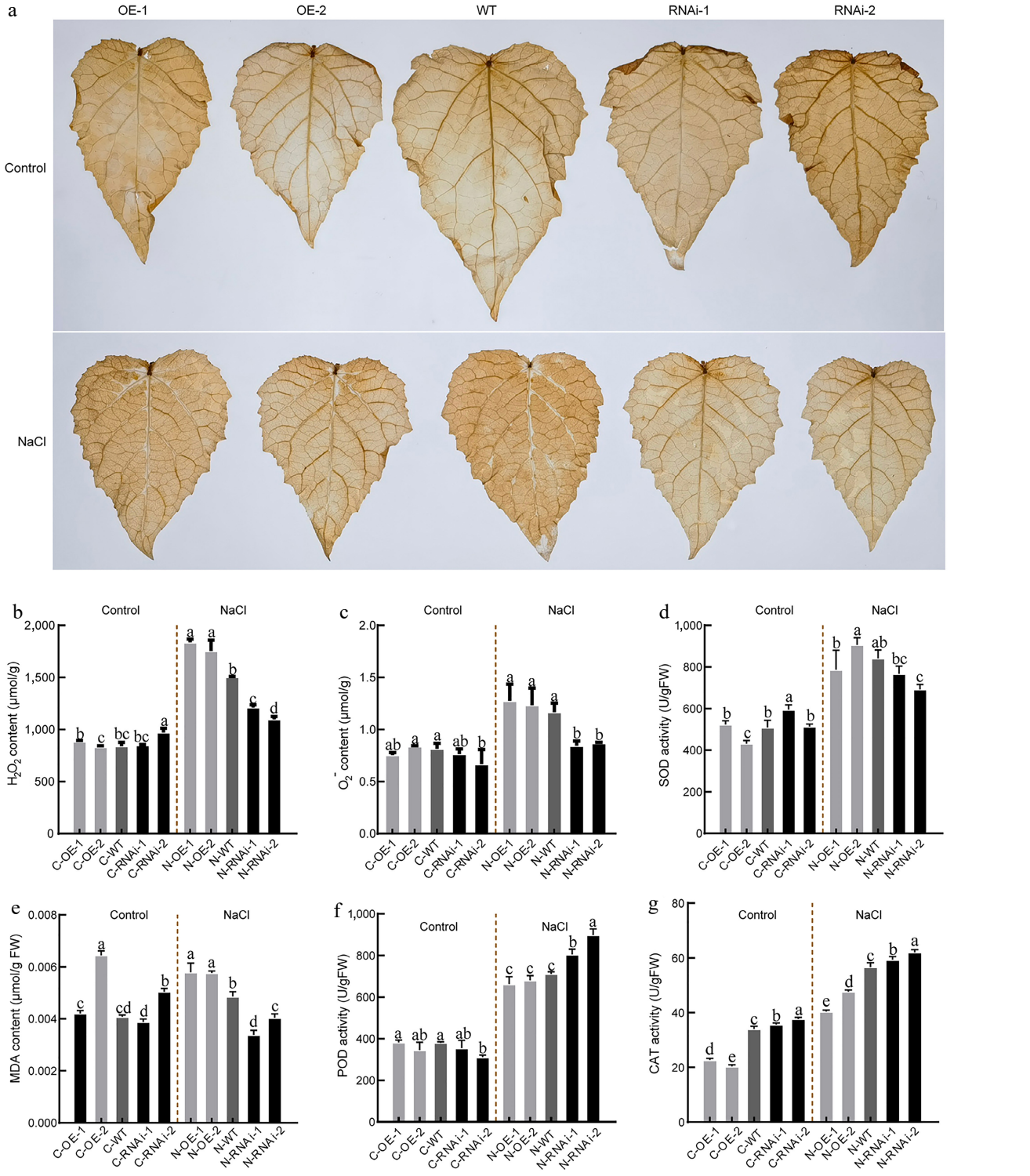

Fig. 5 Antioxidative physiological indices in *PagbZIP60* transgenic poplar under salt stress. (a) Diaminobenzidine (DAB) histological staining of the mature functional leaves of *PagbZIP60* transgenic poplar grown in the pots with 150 mM NaCl for 10 d. (b) Hydrogen peroxide (H_2O_2), and (c) superoxide anion O_2^-) content of the mature functional leaves. (d) Superoxide (SOD), (e) malondialdehyde (MDA) content, (f) peroxidase (POD), and (g) catalase (CAT) activities. The different lowercase letters indicate significant differences among samples ($p < 0.05$). The plot represents the mean ± SD ($n = 6$). OE: *PagbZIP60* overexpression lines, RNAi: *PagbZIP60* suppression lines, WT: non-transgenic poplar, C: normal control growth condition, N: salt stress with NaCl condition. C-OE-1 represents overexpression line 1 under normal conditions; N-OE-1 represents the same line under salt stress. The same nomenclature applies to other abbreviations.

highest, which suggested impaired Na^+ export capacity (Fig. 6g). Specifically, OE lines had the lowest K^+/Na^+ ratio, suggesting that PagbZIP60 mediated ion imbalance and impaired osmotic regulation in poplar.

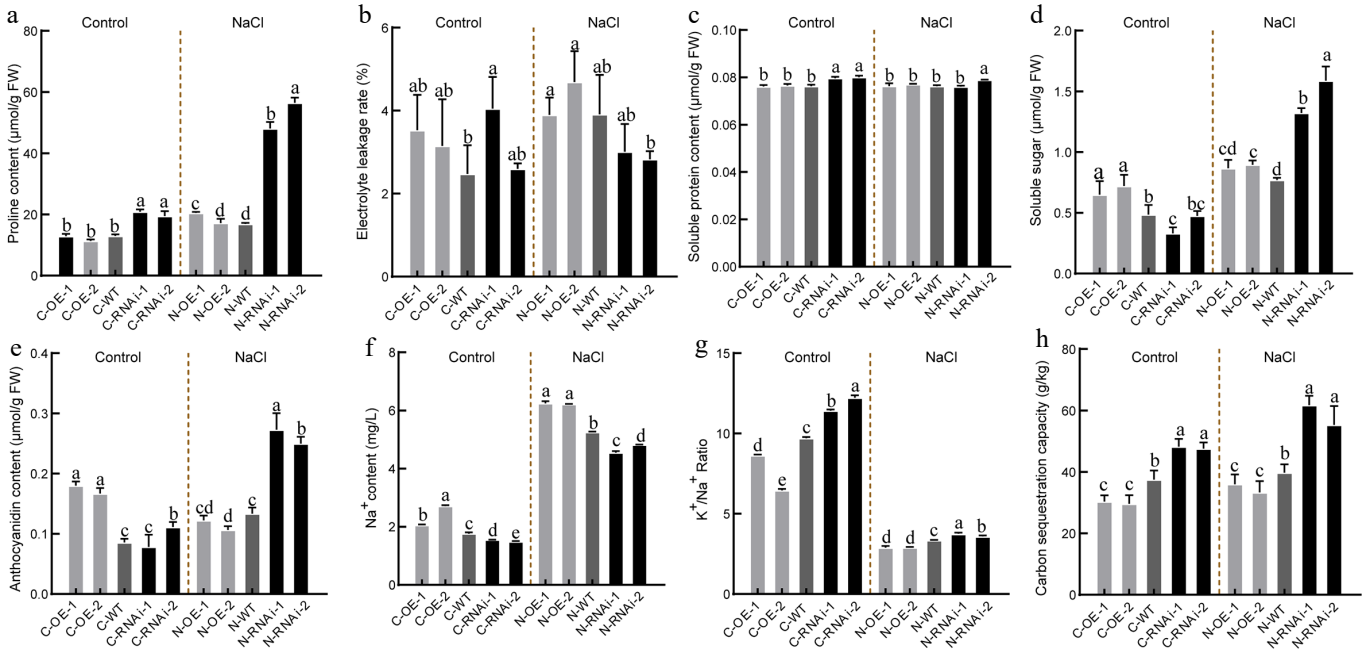

Fig. 6 Osmotic regulation, ion balance and carbon fixation capacity under salt stress in *PagbZIP60* transgenic poplar. (a) Proline content, (b) electrolyte leakage, (c) soluble protein content, (d) soluble sugar content, and (e) anthocyanins content. (f) The contents of Na^+ and (g) ratio of K^+ to Na^+. (h) Carbon sequestration capacity of whole plants detected by 20 biological replicates per line. The different lowercase letters indicate significant differences among samples ($p < 0.05$). The plot represents the mean ± SD ($n = 6$). OE: *PagbZIP60* overexpression lines, RNAi: *PagbZIP60* suppression lines, WT: non-transgenic poplar, C: normal control growth condition, N: salt stress with NaCl condition. C-OE-1 represents overexpression line 1 under normal conditions; N-OE-1 represents the same line under salt stress. The same nomenclature applies to other abbreviations.

PagbZIP60 limited carbon assimilation capacity

To explore the function of PagbZIP60 in carbon sequestration, we compared TOC contents among transgenic lines. Under non-salt conditions, OE lines showed the lowest carbon sequestration capacity, whereas RNAi lines exhibited significantly higher capacity compared to WT (Fig. 6h). Under salt stress, this trend persisted, with RNAi lines exhibiting a further increase in carbon sequestration capacity. To further elucidate how PagbZIP60 regulates poplar carbon sequestration, we analyzed leaf photosynthesis. Stomatal morphology analysis showed that under normal conditions, OE lines had significantly lower stomatal density than WT and RNAi lines, respectively. However, under salt stress, OE lines exhibited higher stomatal density and larger stomatal apertures compared with WT and RNAi lines (Fig. 7a–c). During salt stress, net photosynthetic rates declined in all lines after 3 d (Fig. 7d). From day 6, however, RNAi lines maintained a higher photosynthetic rate but lower transpiration rate compared with WT, which indicated elevated WUE in RNAi lines (Fig. 7e, f). Additionally, OE lines exhibited higher stomatal conductance compared with WT, whereas RNAi lines displayed a lo, wer level during the first 6 d of treatment (Fig. 7g). These results demonstrated that PagbZIP60 suppression enhanced photosynthetic efficiency and reduced transpiration rates, thereby establishing a mechanistic link between improved photosynthetic performance and elevated carbon sequestration capacity in poplar.

Analysis of stem anatomy revealed that under control conditions, the wood fiber lengths in the OE-1 and OE-2 lines were shorter by approximately 4.84% and 0.55% relative to WT (Fig. 7h, i), but those in RNAi-1 and RNAi-2 lines were approximately 4.83% and 0.18% longer, respectively. This pattern remained stable under salt stress. Unfortunately, none of these differences achieved statistical significance, and paraffin section analysis of stem cross-section revealed no significant differences among lines (Supplementary Fig. S4).

PagbZIP60 participated in antioxidant biological processes

RNA-Seq analysis of leaves from OE and WT lines revealed 97 upregulated and 197 downregulated DEGs (Supplementary Fig. S5a). KEGG analysis showed that these DEGs participated in various processes, including cellular processes, environmental information processing, and metabolism (Supplementary Fig. S5b). GO analysis indicated significantly enriched terms, such as cellular/metabolic processes, binding/catalytic activities, response to stimulus, development process, negative regulation of biological processes, growth, and antioxidant activity (Supplementary Fig. S5c). Particularly, DEGs like *TT7*, *PMEI*, *MLP*, *SAUR*, *UGT73B*, and *bZIP61* were involved in the carbohydrate metabolism and antioxidant biological processes of poplar. Their expression patterns, verified by RT-qPCR, indicated that PagbZIP60 may negatively regulate these potential target genes (PTGs), except for *UGT73B* (Supplementary Fig. S6a, S6b; Supplementary Table S1).

bZIPs recognize motifs centered on ACGT, known as ABRE and the unfolded protein response element (UPRE)[34]. ABRE and UPRE elements in the promoters of the PTGs were computationally predicted (Supplementary Fig. S6c). The Y1H assay results showed that the interaction between PagbZIP60 and ABRE/UPRE elements supported yeast growth on the 3-AT selection medium, even at reduced yeast concentrations (Fig. 8a). To verify the inhibitory effect of PagbZIP60 on these PTGs via binding to ABRE/UPRE motifs in their promoters, we genetically fused the coding sequence of *PagbZIP60* to the effector vector and constructed a reporter vector containing five tandem repeats of ABRE/UPRE for LUC assay (Fig. 8b). These results demonstrated that PagbZIP60 significantly repressed the downstream reporter gene activity by specifically recognizing and binding to ABRE/UPRE motifs (Fig. 8c, d). Collectively, PagbZIP60 repressed the expression of these PTGs through its

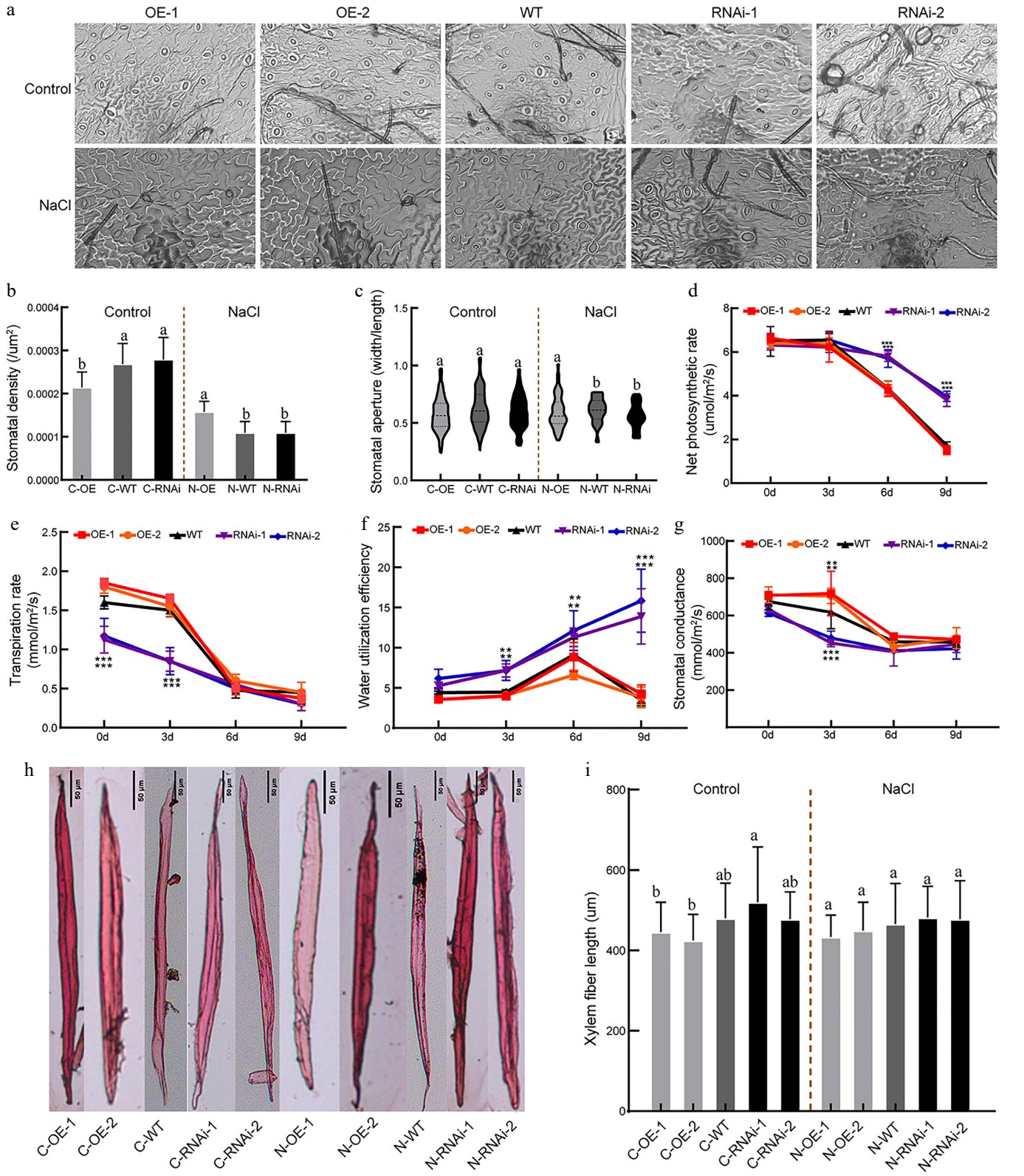

Fig. 7 Photosynthesis indicators and fiber traits of *PagbZIP60* transgenic poplar under salt stress conditions. (a) Stomatal morphology of *PagbZIP60* transgenic poplar. (b) Density, and (c) aperture of open stomata. (d) Net photosynthetic rate, (e) transpiration rate, (f) water utilization efficiency, and (g) stomatal conductance of leaves. (h) Fiber morphology and length of the stems. The different lowercase letters indicate significant differences among samples ($p < 0.05$, [b], [c], [i]). The stars indicate significant differences between *PagbZIP60* transgenic poplar and non-transgenic poplar at the same developmental stage ($p < 0.05$, [d]–[g]). * $p < 0.05$, ** $p < 0.01$, and *** $p < 0.001$. The plot represents the mean ± SD ($n = 6$). OE: *PagbZIP60* overexpression lines, RNAi: *PagbZIP60* suppression lines, WT: non-transgenic poplar, C: normal control growth condition, N: salt stress with NaCl condition. C-OE-1 represents overexpression line 1 under normal conditions; N-OE-1 represents the same line under salt stress. The same nomenclature applies to other abbreviations. Bar: 50 μm.

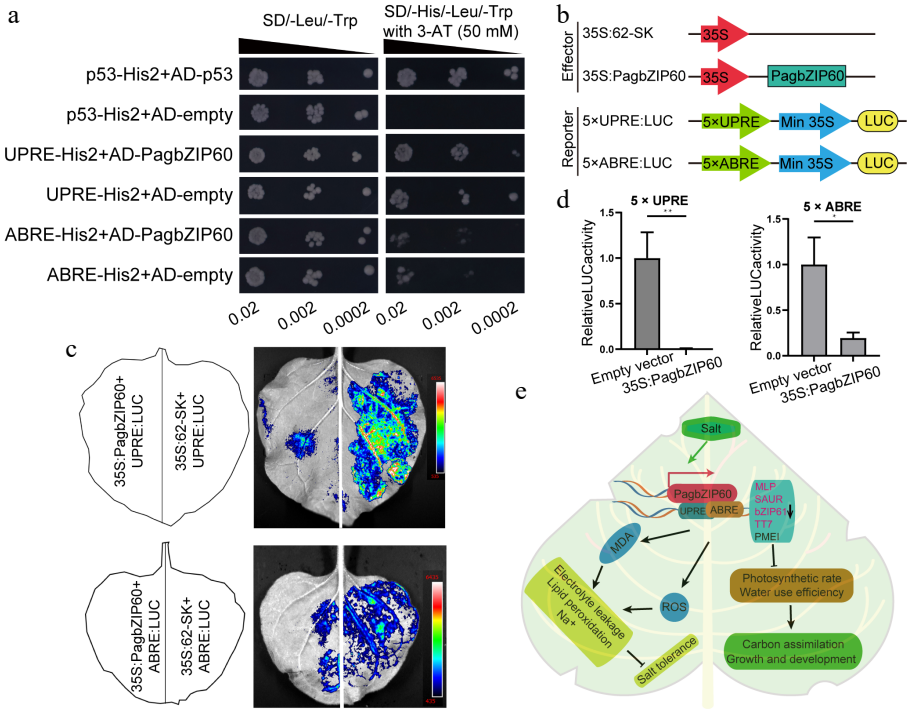

Fig. 8 Downstream targets regulated by PagbZIP60. (a) The binding of PagbZIP60 to UPRE/ABRE motifs was validated using a Y1H assay. Transformed yeast dilutions were plated on synthetic dextrose (SD) media lacking leucine and tryptophan (SD/-Leu/-Trp), and on SD media lacking leucine, tryptophan, and histidine (SD/-His/-Leu/-Trp), with 3-AT (3-amino-1,2,4-triazole). Positive control: p53-His2 + AD-53; Negative control: p53-His2 + AD-empty, UPRE-His2 + AD-empty, ABRE-His2 + AD-empty. (b) *PagbZIP60* and five iterations of *cis*-elements (UPRE/ABRE) were fused to pGreenII 62-SK and pGreenII 0800-LUC vector, respectively. (c) Dual luciferase assays of *PagbZIP60* and (d) *cis*-elements (UPRE/ABRE) by transient expression in tobacco leaves. (e) A model of the mechanism by which PagbZIP60 regulates salt tolerance and carbon assimilation by impairing ROS scavenging and ion homeostasis in poplar. The error bars represent the standard deviation of three biological replicates ($n = 3$). Statistical significance was determined by one-way ANOVA followed by Tukey's post hoc test. Asterisks denote statistically significant differences ($p < 0.05$), * $p < 0.05$, ** $p < 0.01$, *** $p < 0.001$.

interaction with ABRE/UPRE elements in their promoters, thereby regulating growth and antioxidant responses in poplar.

Discussion

Salt stress poses a significant challenge to plant growth and development by severely disrupting the dynamic balance of ions within plant cells, which leads to membrane damage and cell death[35], ultimately interfering with the dynamic balance between ROS accumulation and scavenging within cells[36]. As a consequence, plants experience oxidative stress, which further exacerbates cellular damage. Additionally, the photosynthetic apparatus is adversely affected by salt stress, impairing their ability to efficiently convert light energy into chemical energy[37]. In the context of plant responses to salt stress, bZIPs have emerged as key regulators[14]. In this study, expression pattern analysis revealed that *PagbZIP60* exhibited tissue-specific expression in response to salt stress, suggesting a crucial role in regulating salt tolerance as well as growth and development in poplar.

Growth measurements showed that the vegetative growth, reflected by the plant height and basal stem diameter, was reduced in the OE lines, but RNAi lines displayed the opposite trend compared with WT plants. This aligned with reports that some bZIPs inhibited stem internode elongation[38]. In addition, although *PagbZIP60* was induced by salt stress in the above-ground tissues, its overexpression resulted in greater sensitivity to salt stress. DAB staining revealed that OE leaves accumulated the highest ROS levels (darkest stain), whereas RNAi leaves accumulated the lowest. As antioxidant proteins, SOD, POD, and CAT constitute a primary defense against stress to reduce ROS accumulation[39]. Under salt stress, the activity of the SOD enzyme in OE lines was notably elevated, which may facilitate the dismutation of O_2^- into H_2O_2 and O_2. This, in turn, resulted in an increased concentration of H_2O_2 in OE lines. Meanwhile, comparatively low levels of POD and CAT in OE lines may be insufficient to catalyze the decomposition of H_2O_2 promptly, leading to ROS accumulation and oxidative damage (Fig. 8e). As a secondary metabolite, anthocyanin plays a role in enhancing plant stress tolerance by neutralizing free radicals and mitigating oxidative damage[40]. For example, BoNAC019 reduced anthocyanin accumulation by suppressing the expression of genes involved in anthocyanin synthesis[41]. This reduction in anthocyanin led to an increase in ROS and consequently resulted in a decrease in drought resistance in cabbage flowers. Consistent with this result, OE lines had low levels of anthocyanins, which led to their reduced tolerance to salt stress. Salt stress also damages cell membranes, resulting in the leakage of cellular electrolytes. Meanwhile, MDA, a byproduct of lipid peroxidation, and the rate of electrolyte leakage are both crucial indicators of cell membrane damage[42]. Under such conditions, OE plants demonstrated elevated electrolyte leakage and MDA levels, whereas RNAi lines showed reduced levels of both parameters. These results indicated that PagbZIP60 negatively regulated salt tolerance in poplar by promoting ROS accumulation and lipid peroxidation.

Indeed, under salt stress, an increase in the intracellular Na^+ level can lead to ion imbalance and toxicity within plants[43]. Research has indicated that the expression of certain genes, such as *FcWRKY40*, can enhance the salt tolerance of transgenic plants by preserving

cellular ion homeostasis[44]. AtbZIP62 negatively regulates Na^+ excretion, thereby modulating the antioxidant response and enhancing salt tolerance in *Arabidopsis*[45]. In our study, OE lines exhibited higher Na^+ content, indicating that PagbZIP60 impaired Na^+ efflux, resulting in intracellular Na^+ accumulation. Although this diminished Na^+ efflux strategy can help provide sufficient Na^+ under low-salt conditions, it exacerbates Na^+ toxicity in high-salinity environments. Maintaining the balance between K^+ and Na^+ within cells is critical for plant growth under abiotic stress[46]. A high K^+/Na^+ ratio is beneficial as it can mitigate the toxic effects of Na^+, thus improving salt tolerance[47]. However, OE lines showed a low K^+/Na^+ ratio, indicative of disrupted ion homeostasis. These observations demonstrated that PagbZIP60 negatively regulated salt tolerance in poplar by impairing ion homeostasis, which is a key factor in plant response to saline conditions.

Enhancing afforestation and the carbon sequestration capacity of trees in saline-alkali lands represents a crucial step toward addressing global climate change. Our analysis revealed that under salt-stress conditions, OE lines exhibited higher soluble sugar content than WT plants; however, their ability to sequester carbon was significantly lower than that of WT. These findings demonstrated that OE lines reprogrammed carbon partitioning to accumulate soluble sugars, diverting resources from growth processes to prioritize survival[48]. Conversely, RNAi lines not only had a significantly higher soluble sugar content but also exhibited a superior carbon sequestration capacity. These findings suggested that suppressing the expression of *PagbZIP60* can enhance both the salt tolerance and the carbon sequestration capacity of poplar. The enhancement of plant carbon sequestration capacity is indeed closely linked to photosynthesis, which is the primary process through which plants capture CO_2 and convert it into organic matter[49]. In the context of our study, RNAi lines showed a significant increase in photosynthetic rate and WUE under salt stress, highlighting a physiological mechanism that underlies their enhanced growth and carbon accumulation under saline conditions.

Stomatal movement is regulated by a complex signaling network integrating both endogenous and environmental cues, including the concerted action of signaling proteins, ROS-generating enzymes, and downstream effectors, thereby controlling guard cell turgor[50]. The earliest hallmarks of stomatal closure are ROS accumulation in the apoplast and chloroplasts accompanied by a consecutive rise in cytosolic Ca^{2+} levels, which modulate multiple kinases and regulate ROS-generating enzymes and ion channels[51]. In addition, ROS directly modulates the function of numerous proteins via oxidative post-translational modifications and fine-tuning guard cell signaling[52]. Stomatal regulation of gas exchange between the leaf and atmosphere controls CO_2 uptake for photosynthesis and transpiration, determining plant productivity and WUE[53]. These processes depend on stomatal responses to environmental and internal signals, coordinated with mesophyll CO_2 demands. Consequently, stomatal behavior governs CO_2 diffusion into intercellular air spaces for photosynthesis and plays a critical role in minimizing water loss. In addition, ROS functions in high-CO_2-induced stomatal closure[54]. The reduction in stomatal density and stomatal conductance observed in RNAi lines contributed to the decrease in water loss, a critical adaptation to high-salinity conditions. Furthermore, the larger leaf area and higher leaf number in RNAi lines conferred enhanced light-harvesting capacity, promoting greater photosynthetic biomass production. This dual enhancement of salt tolerance and carbon sequestration capacity makes *PagbZIP60*-suppressed poplar a promising candidate for saline-alkali afforestation.

Notably, our analysis revealed a set of DEGs that were associated with antioxidant activity and carbohydrate metabolism (Supplementary Tables S3, S4). For example, UGT73B, a UDP-glycosyltransferase, affects metabolite stability through modulating the glycosylation of diverse secondary metabolites (e.g., flavonoids, terpenoids), ROS-scavenging capacity, and carbon metabolic flux[55]. Consistent results from Y1H and LUC assays demonstrated that PagbZIP60 directly bound to ABRE/UPRE elements to repress the expression of downstream genes (*TT7*, *PMEI*, *MLP*, *SAUR*, and *bZIP61*). TT7, a key enzyme in flavonoid biosynthesis, catalyzes the formation of secondary metabolites (e.g., anthocyanin) with potent antioxidant activity[56]. In this study, under salt stress conditions, overexpression of *PagbZIP60* inhibited the expression of *TT7*, resulting in reduced anthocyanin accumulation and decreased salt tolerance in OE lines. PMEI modifies cell wall structure by inhibiting pectin methylesterase, influences carbohydrate metabolism and carbon skeleton allocation, processes that are closely linked to carbon sink capacity and cell wall responses to stress[57]. The suppressed expression of *PMEI* observed in OE lines may contribute to the impaired photosynthesis and carbon fixation capacity. Notably, MLP, which participates in MAPK and hormone signaling, serves both as a stress signal transducer and a mediator of ROS signaling[58]. Suppression of *MLP* by PagbZIP60 promoted ROS accumulation in OE lines, consequently reducing their salt tolerance. Furthermore, SAUR participates in salt stress responses, where auxin signaling closely interacts with ROS dynamics and photosynthetic carbon assimilation[59]. It is plausible that in the OE plants, the inhibition of *SAUR* expression may disrupt auxin-mediated ROS/carbon crosstalk, thereby leading to the integrated phenotypes of ROS accumulation, impaired salt tolerance, reduced photosynthetic carbon assimilation, and suppressed growth. Finally, PagbZIP60-mediated suppression of *bZIP61*, a transcription factor implicated in MAPK signaling and stress responses may represent an additional mechanism underlying the reduced salt stress tolerance of OE lines[60]. Collectively, these results indicated that PagbZIP60 played crucial roles in regulating poplar growth and development, as well as adaptation to salt stress.

Conclusions

In this study, a salt stress-induced bZIP transcription factor gene, *PagbZIP60*, was cloned, and its function was characterized (Fig. 8e). Under salt stress, *PagbZIP60* was induced in above-ground tissues and PagbZIP60 bound to ABRE/UPRE elements to repress the expression of downstream genes (*MLP*, *SAUR*, *bZIP61*, *TT7*) associated with antioxidant responses, resulting in elevated ROS levels. The accumulation of ROS led to membrane lipid peroxidation, electrolyte leakage, and increased Na^+ levels. These effects caused oxidative damage and ion imbalance, ultimately reducing salt tolerance. Additionally, the suppression of *PMEI* impaired photosynthesis and water utilization efficiency, thereby reducing carbon assimilation capacity. Collectively, *PagbZIP60* impaired salt tolerance and carbon sequestration capacity by inducing oxidative damage and repressing photosynthesis. Our findings provide a molecular basis for breeding salt-tolerant poplar varieties with enhanced carbon sequestration capacity. These varieties could support targeted afforestation and the improvement of carbon storage in saline-alkali lands.

Author contributions

The authors confirm their contributions to the paper as follows: data curation, investigation, methodology, validation, visualization,

writing – review and editing: Zhang W; data curation, investigation, validation: Li Y; data curation, investigation, validation: Dang H, Wang H; data curation, validation: Du S, Zheng T, Huang J; conceptualization, writing – review and editing: Zhao K; data curation, funding acquisition, investigation, writing – original draft, writing – review and editing: Wang S. All authors reviewed the results and approved the final version of the manuscript.

Data availability

The datasets generated during and/or analyzed during the current study are available from the corresponding author upon reasonable request.

Acknowledgments

This work was supported by the Biological Breeding-National Science and Technology Major Project (2023ZD04056), the Biobreeding Project of Shanxi Agricultural University (YZGC140), the Natural Science Foundation of Shanxi Province (202303021211091), the Shanxi Agricultural University Science and Technology Innovation Fund Project (2014003), the Henan Provincial Natural Science Foundation for Young Scientists (252300421673), and the National-Level Research Project Cultivation Fund Program (XKPY-2022004).

Conflict of interest

The authors declare that they have no conflict of interest.

Supplementary information accompanies this paper online at: https://doi.org/10.48130/forres-0026-0014.

Dates

Received 14 November 2025; Revised 22 February 2026; Accepted 16 March 2026; Published online 14 April 2026

References

[1] Sack L, Buckley TN. 2020. Trait multi-functionality in plant stress response. *Integrative and Comparative Biology* 60:98–112

[2] Zhang H, Zhu J, Gong Z, Zhu JK. 2021. Abiotic stress responses in plants. *Nature Reviews Genetics* 23:104–119

[3] Qiu R, Katul GG. 2020. Maximizing leaf carbon gain in varying saline conditions: an optimization model with dynamic mesophyll conductance. *The Plant Journal* 101:543–554

[4] Fan P, Feng J, Jiang P, Chen X, Bao H, et al. 2011. Coordination of carbon fixation and nitrogen metabolism in *Salicornia europaea* under salinity: comparative proteomic analysis on chloroplast proteins. *Proteomics* 11:4346–4367

[5] Li N, Chen M, Gao X, Long X, Shao H, et al. 2016. Carbon sequestration and *Jerusalem artichoke* biomass under nitrogen applications in coastal saline zone in the northern region of Jiangsu, China. *Science of the Total Environment* 568:885–890

[6] Chen Z, Dayananda B, Fu B, Li Z, Jia Z, et al. 2022. Research on the potential of forestry's carbon-neutral contribution in China from 2021 to 2060. *Sustainability* 14(9):5444

[7] Zhao S, Shi W, Qiao F, Wang C, An Y, et al. 2023. Temporal and spatial changes and trend predictions of forest carbon sequestration efficiency in China based on the carbon neutrality goal. *Forests* 14(12):2387

[8] Ma Z, Cheah WY, Ng IS, Chang JS, Zhao M, et al. 2022. Microalgae-based biotechnological sequestration of carbon dioxide for net zero emissions. *Trends in Biotechnology* 40:1439–1453

[9] Dröge-Laser W, Snoek BL, Snel B, Weiste C. 2018. The *Arabidopsis* bZIP transcription factor family — an update. *Current Opinion in Plant Biology* 45:36–49

[10] Guo Z, Dzinyela R, Yang L, Hwarari D. 2024. bZIP transcription factors: structure, modification, abiotic stress responses and application in plant improvement. *Plants* 13(15):2058

[11] Choi J, Lim CW, Lee SC. 2025. Role of pepper bZIP transcription factor CaADBZ1 in abscisic acid signalling and drought stress response. *Physiologia Plantarum* 177(2):e70159

[12] Li P, Zheng T, Li L, Wang J, Cheng T, et al. 2022. Genome-wide investigation of the bZIP transcription factor gene family in *Prunus mume*: classification, evolution, expression profile and low-temperature stress responses. *Horticultural Plant Journal* 8:230–242

[13] Xu ZY, Kim SY, Hyeon DY, Kim DH, Dong T, et al. 2013. The *Arabidopsis* NAC transcription factor ANAC096 cooperates with bZIP-type transcription factors in dehydration and osmotic stress responses. *The Plant Cell* 25:4708–4724

[14] Zhao K, Chen S, Yao W, Cheng Z, Zhou B, et al. 2021. Genome-wide analysis and expression profile of the bZIP gene family in poplar. *BMC Plant Biology* 21(1):122

[15] Hu J, Nan S, Zhou L, Yu C, Li Y, et al. 2024. PagbZIP75 decreases the ROS accumulation to enhance salt tolerance of poplar via the ABA signaling. *Environmental and Experimental Botany* 228:106051

[16] Henriquez-Valencia C, Moreno AA, Sandoval-Ibañez O, Mitina I, Blanco‐Herrera F, et al. 2015. bZIP17 and bZIP60 regulate the expression of BiP3 and other salt stress responsive genes in an UPR-independent manner in *Arabidopsis thaliana*. *Journal of Cellular Biochemistry* 116:1638–1645

[17] Zhao K, Dang H, Nan S, Yu C, Li Y, et al. 2025. PagHSF4 mediates the biosynthesis of jasmonic acid and plant hormone signal transduction to regulate the growth and development as well as salt stress tolerance of poplar. *Industrial Crops and Products* 234:121582

[18] Wu Y, Hou J, Xiao H, Ye S, Tu D, et al. 2025. OsHDAC1 deacetylates the aldehyde dehydrogenase OsALDH2B1, repressing *OsGR3* and decreasing salt tolerance in rice. *Plant Physiology* 198:kiaf149

[19] Livak KJ, Schmittgen TD. 2001. Analysis of relative gene expression data using real-time quantitative PCR and the $2^{-\Delta\Delta CT}$ method. *Methods* 25:402–408

[20] Shcherbo D, Murphy CS, Ermakova GV, Solovieva EA, Chepurnykh TV, et al. 2009. Far-red fluorescent tags for protein imaging in living tissues. *Biochemical Journal* 418:567–574

[21] He F, Wang HL, Li HG, Su Y, Li S, et al. 2018. PeCHYR1, a ubiquitin E3 ligase from *Populus euphratica*, enhances drought tolerance via ABA-induced stomatal closure by ROS production in *Populus*. *Plant Biotechnology Journal* 16:1514–1528

[22] Wang S, Fan Y, Du S, Zhao K, Liu Q, et al. 2022. PtaERF194 inhibits plant growth and enhances drought tolerance in poplar. *Tree Physiology* 42:1678–1692

[23] Ismail MS, Nawaz F, Shehzad MA. 2025. Contributions of nitrogen metabolic enzymes in storage protein assimilation and mineral accumulation regulated by nitrogen and selenium in *Triticum aestivum* L. *Plant Physiology and Biochemistry* 221:109597

[24] Huang R, Lan T, Song X, Li J, Ling J, et al. 2021. Soil labile organic carbon impacts C:N:P stoichiometry in urban park green spaces depending on vegetation types and time after planting. *Applied Soil Ecology* 163:103926

[25] Xia Y, Han Q, Shu J, Jiang S, Kang X. 2024. Stomatal density suppressor PagSDD1 is a 'generalist' gene that promotes plant growth and improves water use efficiency. *International Journal of Biological Macromolecules* 262:129721

[26] Rueden CT, Eliceiri KW. 2017. The ImageJ ecosystem: an open and extensible platform for biomedical image analysis. *Microscopy and Microanalysis* 23:226–227

[27] Song X, Zhao Y, Wang J, Lu MZ. 2021. The transcription factor KNAT2/6b mediates changes in plant architecture in response to drought via downregulating *GA20ox1* in *Populus alba* × *P. glandulosa*. *Journal of experimental botany* 72:5625–5637

[28] Wang K, Shen X, Williams R. 2021. Sequencing BGI: the evolution of expertise and research organisation in the world's leading gene sequencing facility. *New Genetics and Society* 40:305−330

[29] Kim D, Langmead B, Salzberg SL. 2015. HISAT: a fast spliced aligner with low memory requirements. *Nature Methods* 12(4):357−360

[30] Love MI, Huber W, Anders S. 2014. Moderated estimation of fold change and dispersion for RNA-seq data with DESeq2. *Genome Biology* 15(12):550

[31] Young MD, Wakefield MJ, Smyth GK, Oshlack A. 2010. Gene ontology analysis for RNA-seq: accounting for selection bias. *Genome Biology* 11(2):R14

[32] Wang P, Yang X, Sun S, Wang J, Wang J, et al. 2025. The SCARECROW-LIKE transcription factor from *Populus davidiana* × *P. bolleana* simultaneously improved drought tolerance and plant growth through acetylation - dependent mechanisms. *Plant Biotechnology Journal* 23(9):3650−3666

[33] Chen H, Wu W, Du K, Ling A, Kang X. 2024. The interplay of growth-regulating factor 5 and BZR1 in coregulating chlorophyll degradation in poplar. *Plant, Cell & Environment* 47:3766−3779

[34] Iwata Y, Fedoroff NV, Koizumi N. 2008. *Arabidopsis* bZIP60 is a proteolysis-activated transcription factor involved in the endoplasmic reticulum stress response. *The Plant Cell* 20:3107−3121

[35] Wang P, Guo Q, Wang Q, Zhou XR, Wang SM. 2015. PtAKT1 maintains selective absorption capacity for K^+ over Na^+ in halophyte *Puccinellia tenuiflora* under salt stress. *Acta Physiologiae Plantarum* 37(5):100

[36] Zorov DB, Juhaszova M, Sollott SJ. 2014. Mitochondrial reactive oxygen species (ROS) and ROS-induced ROS release. *Physiological Reviews* 94:909−950

[37] Takahashi S, Murata N. 2008. How do environmental stresses accelerate photoinhibition? *Trends in Plant Science* 13:178−182

[38] Fukazawa J, Sakai T, Ishida S, Yamaguchi I, Kamiya Y, et al. 2000. REPRESSION OF SHOOT GROWTH, a bZIP transcriptional activator, regulates cell elongation by controlling the level of gibberellins. *The Plant Cell* 12:901−915

[39] Mittler R, Vanderauwera S, Gollery M, Van Breusegem F. 2004. Reactive oxygen gene network of plants. *Trends in Plant Science* 9:490−498

[40] Van den Ende W, El-Esawe SK. 2014. Sucrose signaling pathways leading to fructan and anthocyanin accumulation: a dual function in abiotic and biotic stress responses? *Environmental and Experimental Botany* 108:4−13

[41] Wang J, Lian W, Cao Y, Wang X, Wang G, et al. 2018. Overexpression of *BoNAC019*, a NAC transcription factor from *Brassica oleracea*, negatively regulates the dehydration response and anthocyanin biosynthesis in *Arabidopsis*. *Scientific Reports* 8:13349

[42] Baxter A, Mittler R, Suzuki N. 2014. ROS as key players in plant stress signalling. *Journal of Experimental Botany* 65:1229−1240

[43] Huang GT, Ma SL, Bai LP, Zhang L, Ma H, et al. 2012. Signal transduction during cold, salt, and drought stresses in plants. *Molecular Biology Reports* 39:969−987

[44] Dai W, Wang M, Gong X, Liu JH. 2018. The transcription factor FcWRKY40 of *Fortunella crassifolia* functions positively in salt tolerance through modulation of ion homeostasis and proline biosynthesis by directly regulating *SOS2* and *P5CS1* homologs. *New Phytologist* 219:972−989

[45] Rolly NK, Imran QM, Lee IJ, Yun BW. 2020. Salinity stress-mediated suppression of expression of salt overly sensitive signaling pathway genes suggests negative regulation by *AtbZIP62* transcription factor in *Arabidopsis thaliana*. *International Journal of Molecular Sciences* 21(5):1726

[46] Tian Q, Shen L, Luan J, Zhou Z, Guo D, et al. 2021. Rice shaker potassium channel OsAKT2 positively regulates salt tolerance and grain yield by mediating K^+ redistribution. *Plant, Cell & Environment* 44:2951−2965

[47] Wang Z, Hong Y, Zhu G, Li Y, Niu Q, et al. 2020. Loss of salt tolerance during tomato domestication conferred by variation in a Na^+/K^+ transporter. *The EMBO Journal* 39(10):EMBJ2019103256

[48] Huang J, Hammerbacher A, Gershenzon J, van Dam NM, Sala A, et al. 2021. Storage of carbon reserves in spruce trees is prioritized over growth in the face of carbon limitation. *Proceedings of the National Academy of Sciences of the United States of America* 118(33):e2023297118

[49] Gang H, Li R, Zhao Y, Liu G, Chen S, et al. 2019. Loss of GLK1 transcription factor function reveals new insights in chlorophyll biosynthesis and chloroplast development. *Journal of Experimental Botany* 70:3125−3138

[50] Sierla M, Waszczak C, Vahisalu T, Kangasjärvi J. 2016. Reactive oxygen species in the regulation of stomatal movements. *Plant Physiology* 171:1569−1580

[51] Marten H, Konrad KR, Dietrich P, Roelfsema MRG, Hedrich R. 2007. Ca^{2+}-dependent and -independent abscisic acid activation of plasma membrane anion channels in guard cells of *Nicotiana tabacum*. *Plant Physiology* 143:28−37

[52] Qi J, Song CP, Wang B, Zhou J, Kangasjärvi J, et al. 2018. Reactive oxygen species signaling and stomatal movement in plant responses to drought stress and pathogen attack. *Journal of Integrative Plant Biology* 60:805−826

[53] Lawson T, Blatt MR. 2014. Stomatal size, speed, and responsiveness impact on photosynthesis and water use efficiency. *Plant Physiology* 164:1556−1570

[54] Chater C, Peng K, Movahedi M, Dunn JA, Walker HJ, et al. 2015. Elevated CO_2-induced responses in stomata require ABA and ABA signaling. *Current Biology* 25:2709−2716

[55] Simon C, Langlois-Meurinne M, Didierlaurent L, Chaouch S, Bellvert F, et al. 2014. The secondary metabolism glycosyltransferases UGT73B3 and UGT73B5 are components of redox status in resistance of *Arabidopsis* to *Pseudomonas syringae* pv. *tomato*. *Plant, Cell & Environment* 37:1114−1129

[56] Han Y, Vimolmangkang S, Soria-Guerra RE, Rosales-Mendoza S, Zheng D, et al. 2010. Ectopic expression of apple *F3'H* genes contributes to anthocyanin accumulation in the *Arabidopsis tt7* mutant grown under nitrogen stress. *Plant Physiology* 153:806−820

[57] Röckel N, Wolf S, Kost B, Rausch T, Greiner S. 2008. Elaborate spatial patterning of cell-wall PME and PMEI at the pollen tube tip involves PMEI endocytosis, and reflects the distribution of esterified and de-esterified pectins. *The Plant Journal* 53:133−143

[58] Ruperti B, Bonghi C, Ziliotto F, Pagni S, Rasori A, et al. 2002. Characterization of a major latex protein (MLP) gene down-regulated by ethylene during peach fruitlet abscission. *Plant Science* 163:265−272

[59] Ren H, Gray WM. 2015. SAUR proteins as effectors of hormonal and environmental signals in plant growth. *Molecular Plant* 8:1153−1164

[60] Shen YY, Wang XF, Wu FQ, Du SY, Cao Z, et al. 2006. The Mg-chelatase H subunit is an abscisic acid receptor. *Nature* 443:823−826